REPORT DOCUMENTATION PAGE

1. REPORT DATE (DD-MM-YYYY)	2. REPORT TYPE	3. DATES COVERED (From - To)
27-12-02	Technical Paper	

4. TITLE AND SUBTITLE	5a. CONTRACT NUMBER
Numerical Cold Flow and Combustion Characterization of Swirl Coaxial Injectors	5b. GRANT NUMBER
	5c. PROGRAM ELEMENT NUMBER

6. AUTHOR(S)	5d. PROJECT NUMBER
Jeffrey A. Muss, Curtis W. Johnson[1] Gary C. Cheng[2]	3058
	5e. TASK NUMBER
	RF9A
	5f. WORK UNIT NUMBER

7. PERFORMING ORGANIZATION NAME(S) AND ADDRESS(ES)	8. PERFORMING ORGANIZATION REPORT NUMBER
[1]Sierra Engineering, Inc. Carson City, NV [2]University of Alabama Birmingham Birmingham, AL	AFRL-PR-ED-TP-2002-323

9. SPONSORING / MONITORING AGENCY NAME(S) AND ADDRESS(ES)	10. SPONSOR/MONITOR'S ACRONYM(S)
Air Force Research Laboratory (AFMC) AFRL/PRS 5 Pollux Drive Edwards AFB CA 93524-7048	11. SPONSOR/MONITOR'S NUMBER(S) AFRL-PR-ED-TP-2002-323

12. DISTRIBUTION / AVAILABILITY STATEMENT

Approved for public release; distribution unlimited.

13. SUPPLEMENTARY NOTES

14. ABSTRACT

20030227 156

15. SUBJECT TERMS

16. SECURITY CLASSIFICATION OF:			17. LIMITATION OF ABSTRACT	18. NUMBER OF PAGES	19a. NAME OF RESPONSIBLE PERSON Leilani Richardson
a. REPORT	b. ABSTRACT	c. THIS PAGE	A		19b. TELEPHONE NUMBER (include area code) (661) 275-5015
Unclassified	Unclassified	Unclassified			

3058RF9A

MEMORANDUM FOR PRS (Contractor Publication)

FROM: PROI (STINFO)   27 Dec 2002

SUBJECT: Authorization for Release of Technical Information, Control Number: **AFRL-PR-ED-TP-2002-323**
Jeff Muss (Sierra Engineering) et al., "Numerical Cold Flow and Combustion Characterization of Swirl /
Coaxial Injectors"

AIAA Aerospace Sciences Conference   **(Statement A)**
(Reno, NV, 6-9 January 2003) (Deadline: 06 Jan 2003)

Numerical Cold Flow and Combustion Characterization of Swirl Coaxial Injectors

916-363-6161   ← Jeffrey A. Muss* and Curtis W. Johnson# →   775-885-0139

Coll   r956-6557

Sierra Engineering, Inc.
Carson City, NV

Gary C. Cheng*
University of Alabama Birmingham,
Birmingham, AL

Richard K. Cohn#
Air Force Research Laboratory,
Edwards AFB, CA

Abstract

The Air Force and its partners are developing and validating an injector design methodology that utilizes both high-pressure cold-flow testing and uni-element hot-fire testing, to create a high performing, long life swirl coaxial injector. Several gas-centered swirl coax injector configurations have been tested under cold-flow and hot-fire test conditions in a single element research engine. The methodology uses computational fluid dynamics (CFD) analyses to provide insight into the flowfield and guide the evolution of injector designs. Both cold-flow and hot-fire analyses were completed, with cold flow results compared with test data. The companion paper will discuss the experimental results.

Introduction

Proper injector design is critical to achieving long engine life while providing high combustion efficiency in rocket combustion chambers. Gas-centered swirl coaxial injectors, which swirl liquid fuel around a gaseous oxygen core, show promise for the next generation hydrocarbon fueled staged-combustion rocket engines. Introducing a swirl component in the injector flow can enhance the propellant mixing and thus improve engine performance. These injectors can be designed with large element thrusts, reducing manufacturing costs, while providing good spatial uniformity and a low face temperature, both of which improve engine life.

Sierra Engineering and the Air Force Research Laboratory (AFRL) have undertaken a program to develop design guidelines for gas-centered swirl coaxial injectors. The element will initially be used in an Alternate Fuels Testbed (AFT) combustor to test hydrocarbon fuel performance and operability. In order to produce meaningful results, the 2000 lbf thrust multi-element AFT combustor has to be high performing and adaptable to different hydrocarbon based fuels. The combustor operates on ambient temperature gaseous oxygen and an array of fuels. The combustor is designed with removable injector elements, allowing the element geometry to be tailored for each fuel if it proves necessary.

The basic gas-centered swirl coaxial element design can be conceptualized as a straight-run post for the oxidizer (Figure 1). The post includes a discrete set of fuel injection orifices near the downstream exit of the oxidizer post. The orifices are oriented to generate swirling fuel around the periphery. The fuel film generated around the post periphery is subject to a combination of cross-flow shear and centrifugal forces. As the liquid exits the tip of the oxidizer post, centrifugal forces create a conically expanding sheet of liquid that thins due to continuity. This liquid sheet film also interacts with the central oxygen gas jet, which typically entrains the liquid fluid and transports the resultant spray downstream. The parameters that can be varied in this design include the number of fuel injection orifices, the axial location of the orifices relative to the final injection location and most importantly the post geometry near the fuel injection orifices.

Three basic injector concepts were identified for comparative evaluation, the diverger, the converger and the pre-filmer, as shown schematically in Figure 2

and discussed in more detail in Reference 1. Each element concept was first cold flow tested in the high pressure injector rig at AFRL. Many of the elements have also undergone extensive hot-fire testing in AFRL's EC-1 facility. The final phase of this program will be hot-fire testing of the multi-element AFT combustor at AFRL's 1-14 test facility.

The companion computational fluid dynamics (CFD) analysis effort has been used to gain insight into the physics and the trends for different designs of the swirl coaxial elements. Uni-element cold flow and hot-fire analyses, and limited multi-element hot-fire simulations have been completed. This paper discusses the CFD solutions for the various hardware configurations and compares the simulation results to available cold flow test data.

The Gas-Centered Swirl Coaxial Element

Figure 1 shows a cut-away of the simple gas-centered swirl coaxial element. Unlike shear-coaxial elements commonly used in hydrogen-oxygen rocket engines, the subject design uses only a single wall to separate fuel and oxidizer flows and direct the fluids to the injection location. Gaseous oxygen flows through the center of the element (GOX post). No swirl component is imparted to the oxidizer in these designs. The fuel is injected tangentially at three or four ports uniformly spaced around the GOX inner diameter. The fuel then swirls along the GOX post wall, creating a sheet, which subsequently interacts with the core oxidizer and swept out of the element. Figure 1 shows a GOX post with a sudden expansion and a divergent cone at the tip (a "diverger"). Several different tip geometries have been fabricated and tested (see Figure 2 and Reference 1).

Numerical Models

The present study employed a finite difference Navier-Stokes (FDNS) CFD flow solver to analyze the flowfield within and emanating from these gas-liquid swirl injectors[1-4]. A homogeneous spray approach with a real-fluid property submodel was incorporated into the FDNS solver (FDNS-RFV) to simulate liquid spray phenomena. In the present real-fluid model, thermal and caloric equations of state, vapor pressure, heat of vaporization, surface tension, and transport properties are modeled with the equations of state (EOS) proposed by Hirshfelder, et al.[6-7] (we term these the HBMS equations of state), while conventional correlations[8] are used for the other properties.

Mixture properties are calculated by using the additive volume method when multi-component fluid/vapor mixtures are present in the flowfield. This means that multiphase mixtures are treated as ideal solutions. When the mixture is under conditions where the species become ideal gases, the thermodynamic data from the CEC code[9] is used.

The FDNS code has been widely employed by NASA MSFC to analyze various flow problems of rocket engines. The framework of the FDNS-RFV code is an elliptic finite difference Navier-Stokes flow solver employing a predictor plus a multi-corrector pressure-based solution algorithm. Higher order upwind, total variation diminishing (TVD) or central difference schemes plus adaptive second-order and fourth-order dissipation terms are used to approximate the convection terms of the transport equations. Various matrix solvers, such as vectorized point implicit, conjugate gradient, and generalized minimal residual (GMRES), are provided in the code so that users can select one for a given transport equation[10]. Since the FDNS-RFV flow solver is a structured code, multi-block, multi-zone options are included to enable efficient analysis of problems with complex geometries. In order to properly account for the compressibility effects with a homogeneous spray model, the sound speed of a multi-component mixture was calculated using the real-fluid property submodel.
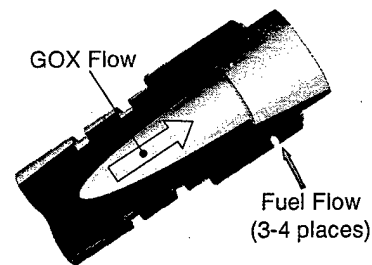

Figure 1: Schematic Cross-Section of Gas-Centered Swirl Coaxial Element

The current homogeneous spray model has been used to simulate single element like-on-like (LOL) and unlike doublet impinging element cold-flow experiments. The numerical results show reasonable agreement with the analytical results[4]. Recently, the homogeneous spray model was employed to simulate cryogenic nitrogen injections and spray combustion of GH2/LO2 shear coaxial injectors. The comparisons of the numerical results with the test data were extremely

2

successful[2]. Hence, the homogeneous spray model was deemed acceptable for the analysis of gas-liquid swirl injectors. It should be noted that this model assumes the particulate phase and the gas phase to be in equilibrium, thus it is most suitable for mixing at supercritical and near critical conditions. The cold flow tests utilize sub-critical water injection that is expected to result in some inaccuracies.

A finite-rate chemistry model was employed in the hot-fire simulations to capture the significant coupling between the fluid mechanics and chemical reactions with O_2/RP-1 propellants. This kinetic model[4] includes RP-1 pyrolysis, soot formation, soot oxidation, pyrolysis gas oxidation, and wet-CO mechanism (

Table 1). The kinetic model was developed and validated using experimental rocket engine data for soot concentration as a function of oxidizer-to-fuel mixture ratio[11].

CFD Simulation Details

Three series of progressively more complex CFD simulations were conducted in parallel with experimental test programs. The first and simplest series simulated non-reacting cold flow mixing between water and gaseous nitrogen for a single swirl coaxial element enclosed in a pressurized vessel. The second series evaluated reacting hot-fire single element operation using gaseous oxygen and RP-1 as propellants. The final series simulated hot-fire operation of the 5 element AFT combustor with RP-1 and gaseous as propellants. This section describes the various configurations in more detail.

Simulations were performed for cold flow injector operation of a single injection element for three injector configurations (Injector #4, #7, and #11 shown in Figure 2), representing each of the basic injector types considered. Operation was simulated at two operating chamber pressures (Pc = 271 psig and 842 psig). Studying different injector configurations helped elucidate the effect of geometry on the propellant atomization and mixing, while evaluation of different operating conditions reveals the trend of the propellant mixing with chamber pressure. Water was used as the fuel simulant and gaseous nitrogen as the oxidizer simulant in both the cold flow tests and the CFD calculations. The numerical results for various cases are compared to the test data in the following section.

The operating condition, boundary conditions, and injector geometry in a typical cold flow numerical simulation are illustrated in Figure 3. The element cold flow testing was performed in a pressurized container with the element situated within the pressure vessel[11]. An entrainment boundary condition is used to simulate the cavity region outside of the injector faceplate. The injectors containing three fuel injection holes were modelled with a 120° pie section while four hole injectors are modeled with a 90° pie section. The computational domain is represented using a two-zone mesh system. The injector section, designated as the first zone, consists of approximately a 45 x 31 x 43 grid system; while the second zone, employed to model the pressurized plenum section, used approximately a 71 x 101 x 43 mesh system. Exact grid dimensions depended uoon the geometry.
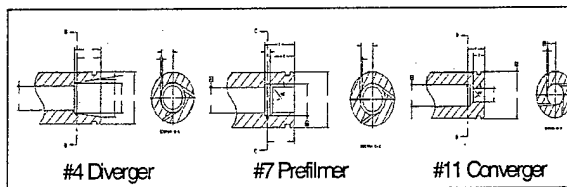

#4 Diverger   #7 Prefilmer   #11 Converger

Figure 2: Basic Injector Geometry Types

Hot-fire uni-element simulations were also performed for Injector #11. The simulation considered operation at a chamber pressure of 825 psig with gaseous O_2 as the oxidizer and RP-1 as the fuel. The operating condition, boundary conditions, and injector geometry are depicted in Figure 4. Uni-element hot-fire testing was performed with a sonic throat, however the simulation considers only the cylindrical portion of the test article, with the downstream boundary pressure imposed. Only a 90° pie section of the flowfield was modeled.
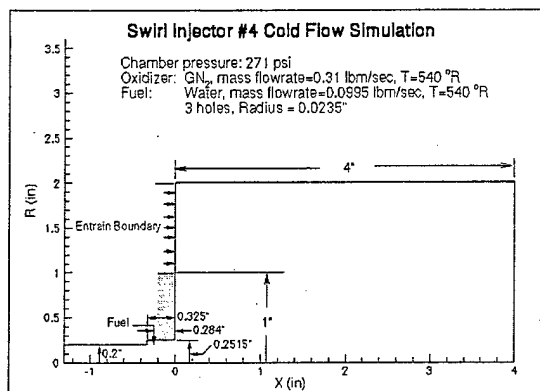
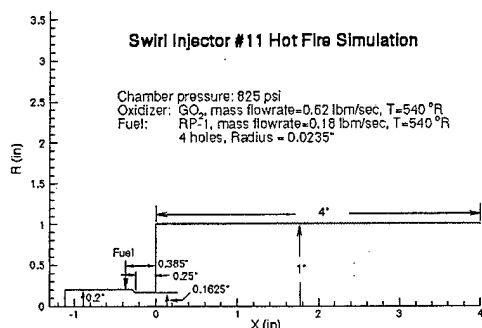**Figure 3: Flow and Boundary Conditions of a Typical Numerical Cold Flow Simulation**

Figure 4: Computational Boundaries for Hot-Fire Uni-Element Simulation

Hot-fire simulations with gaseous O_2 as the oxidizer and RP-1 as the fuel were also performed for the 5-element AFT engine at operating pressures of 1000 and 2000 psi. Injector #11 was used as the injection element. As a result of the non-axisymmetric nature of the injection element, a 72° pie section of the engine, encompassing a complete element, was modeled (Figure 5). The operating condition, boundary conditions, and simulated engine geometry are depicted in Figure 6. Although the AFT engine includes a sonic throat, the simulation considers only the cylindrical portion of the test article, with the downstream boundary pressure imposed.
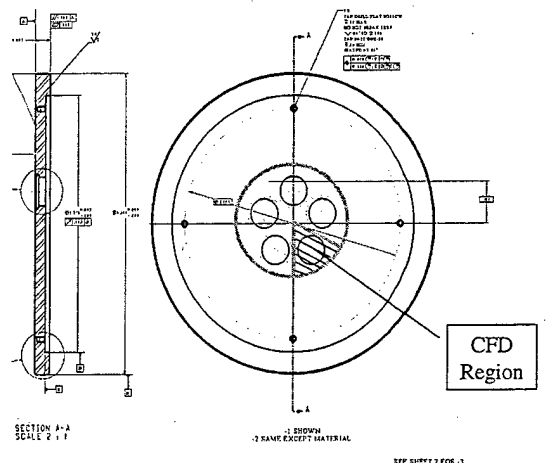

Figure 5: Depiction of Injector Face Computational Boundary used in AFT Hot-Fire Simulations

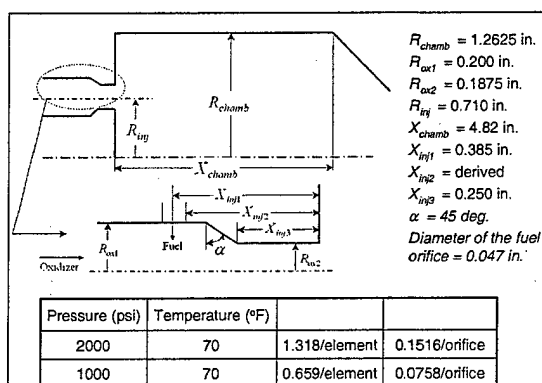| Pressure (psi)	Temperature (°F)		
2000	70	1.318/element	0.1516/orifice
1000	70	0.659/element	0.0758/orifice

Figure 6: Flow and Boundary Conditions used for AFT Hot-Fire Simulations

<u>Uni-element Cold Flow Results</u>

CFD solutions for the cold flow simulations are presented in this section. The interpretation of the results is contained in a subsequent section. The results for each of the three injectors studied are presented side-by-side where possible to afford easy comparisons.

Fuel mass fraction distributions are presented at three azimuthal planes for Injectors #4, #7 and #11 in Figure 7 through Figure 9, while planar slices across the spray are presented at several axial stations in Figure 10 through Figure 12. The improved flowfield circumferential symmetric of Injector #11 is readily evident.

4

Circumferentially-averaged fuel mass flux distributions are plotted at several axial stations in Figure 13 through Figure 15 for each of the injectors. The radial spread of the fuel mass, both outward towards the freestream as well as inward into the central oxidizer core is clearly visible shortly after the spray leaves the injector. It is interesting to note that by an axial station of x=2.0 inches most of asymmetries resulting from discrete fuel injection are mixed-out for the pre-filmer design (#7) and the converging design (#11). However, these asymmetries persist until an axial station of X=4.0 inches for the diverging design (#4). This behavior could produce circumferentially non-uniform thermal loads in the combustion chamber if these trends persist in the hot-fire tests. The fuel mass flux predicted two inches downstream from the injector exit are compared to test data for each of the injectors (Figure 16-Figure 18). It is obvious that there are discrepancy in the absolute value of the mass flux between the numerical result and the test data. This discrepancy is likely caused by the low total water flow collection efficiency detected during patternator measurements. Poor total fuel (water) collection efficiency was a persistent problem throughout the cold flow test program[1].

Fuel streamlines emanating from a single fuel orifice are displayed in Figure 19 through Figure 21. It can be seen that the fuel film retains a large tangential motion for the diverger and pre-filming elements. The converger element design, however, produces a strong interaction between the core gas flow and the injected fuel, resulting in transition to nearly axial fuel flow within the injection element.

Uni-element Hot-Fire Results

Uni-element hot-fire simulation was only performed for converger Injector #11, and only at a single operating condition (Pc=825 psi). Planar temperature profiles taken at several azimuthal stations indicate good circumferential symmetry along the length of the combustion chamber (Figure 22). Transverse slices across the chamber at various axial stations reveal only a slight asymmetry, and this persists only very near the injector (Figure 23). Streamline traces of the fuel emanating from a single orifice rapidly transitions to pure axial flow (Figure 24); this behavior is very similar to that predicted during cold flow element operation (Figure 21).

Multi-Element Hot-Fire Results

Hot-fire reacting flow predictions were performed for the multi-element AFT combustor at chamber pressures of both 1000 and 2000 psi. Significant differences in the combustion flowfield are clearly visible. Computer hardware limitations resulted in a grid system that was not sufficient to resolve the steep gradients at the reaction front, but the location of the reaction zone is readily identifiable.

Temperature and velocity fields across the center of an injection element are shown for both cases in Figure 25 and Figure 28. Significant reaction occurs within the injection element and the main chamber flow is distorted for the 1000 psi case (Figure 25) while the reaction is stabilized at the element exit for the 2000 psi case (Figure 28). The flowfield in the combustion chamber is also much more one-dimensional for the high pressure case. Close-up views of the injector outlet temperature (Figure 26 and Figure 29) and the oxidizer mass fraction (Figure 30 and Figure 27) reinforce these observations.

Radial temperature (Figure 31 and Figure 33) and oxidizer-to-fuel mass mixture ratio (MR) (Figure 32 and Figure 34) are presented for both operating conditions. Both sets of profiles are much more uniform, both axially and radially for the low pressure (1000 psi) operating condition. This is somewhat incongruous with the temperature contours presented in Figure 25and Figure 28.

American Institute of Aeronautics and Astronautics

Fuel Concentrations at Various Circumferential Planes (Inj. #4)
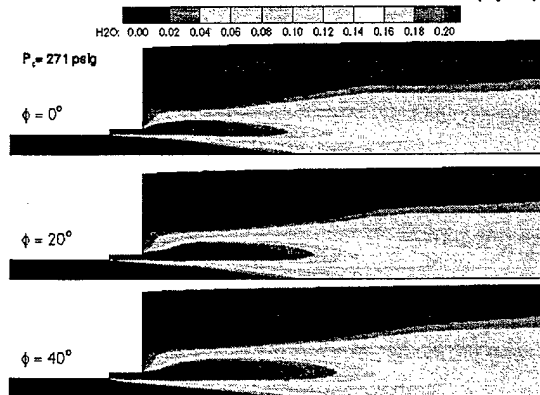
Figure 7: Fuel Mass Fraction Contours for Various
Circumferential Planes for Diverger Injector #4

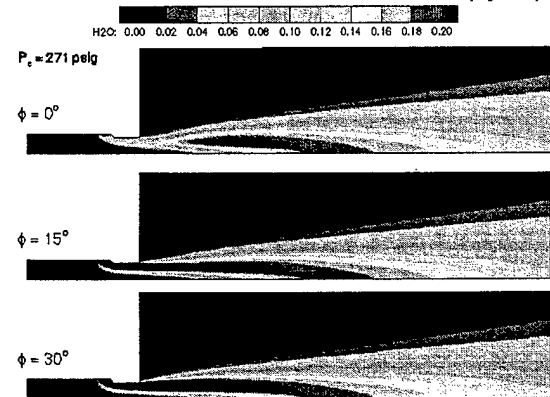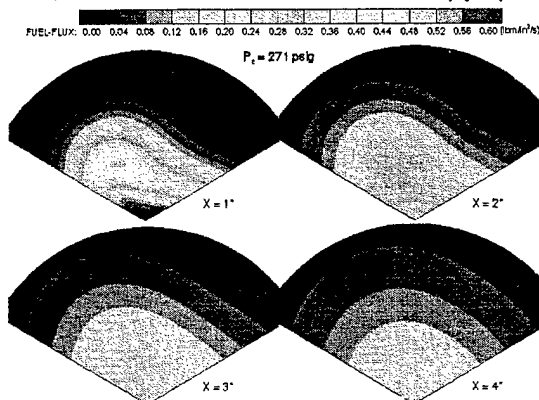Fuel Mass Flux Profiles at Various Axial Locations (Inj. #4)

Figure 10: Fuel Mass Flux Contours at Various
Axial Locations for Injector #4

Fuel Concentrations at Various Circumferential Planes (Inj. #7)
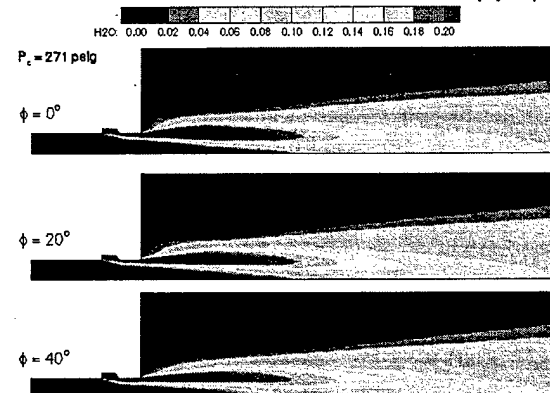
Figure 8: Fuel Mass Fraction Contours for Various
Circumferential Planes for Pre-filming Injector #7

Fuel Mass Flux Profiles at Various Axial Locations (Inj. #7)
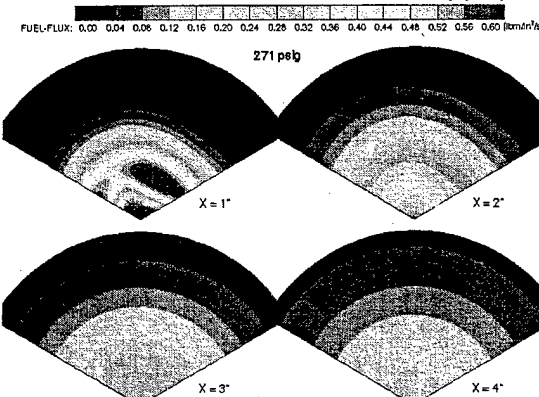
Figure 11: Fuel Mass Flux Contours at Various
Axial Locations for Injector #7

Fuel Concentrations at Various Circumferential Planes (Inj. #11)

Figure 9: Fuel Mass Fraction Contours at Various
Circumferential Planes Converging Injector #11
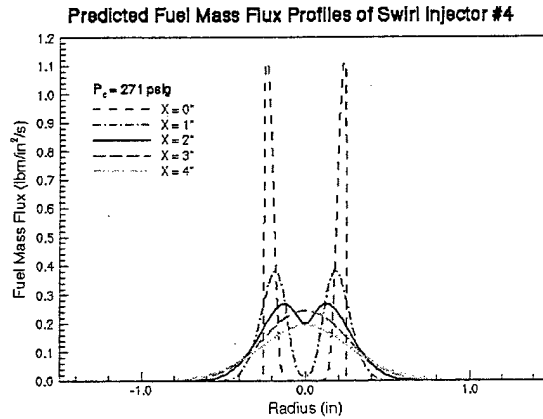
Fuel Mass Flux Profiles at Various Axial Locations (Inj. #11)
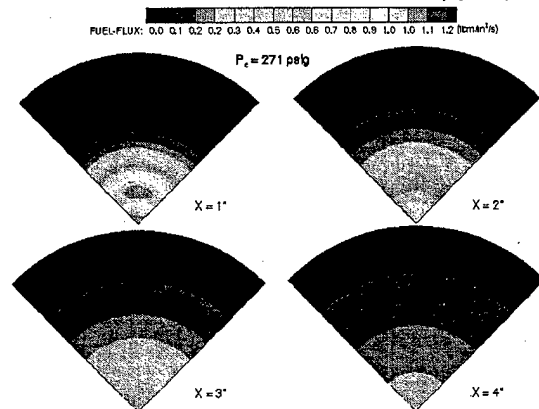
Figure 12: Fuel Mass Flux Contours at Various
Axial Locations for Injector #11

6

Predicted Fuel Mass Flux Profiles of Swirl Injector #4

Figure 13: Averaged Fuel Mass Flux Profile at Various Axial Locations for Injector #4

Comparison of Fuel Mass Flux Distribution of Swirl Injector #4
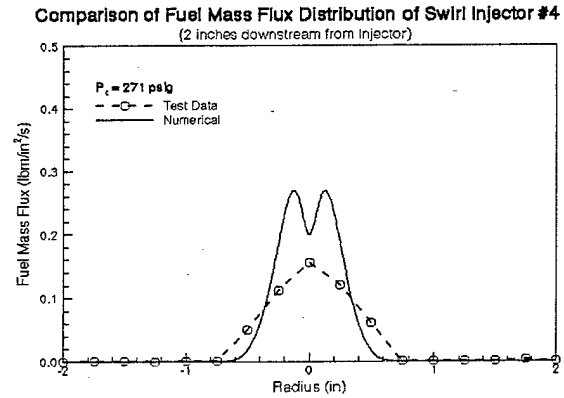(2 inches downstream from Injector)

Figure 16: Comparison of Averaged Fuel Mass Flux Computations and Measurements 2-inches Downstream of Injector #4

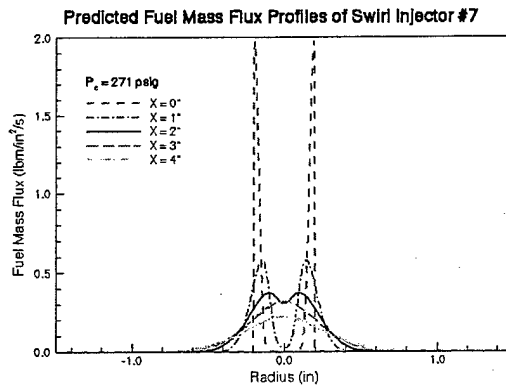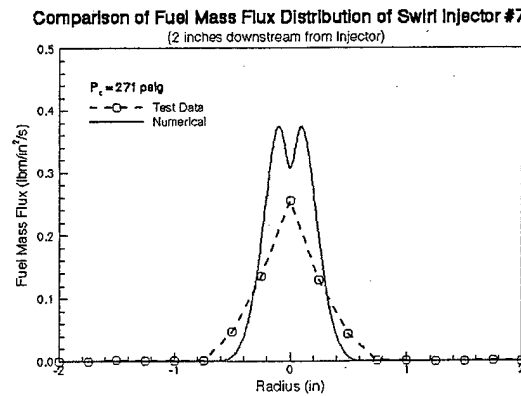**Predicted Fuel Mass Flux Profiles of Swirl Injector #7**

Figure 14: Averaged Fuel Mass Flux Profile at Various Axial Locations for Injector #7

Comparison of Fuel Mass Flux Distribution of Swirl Injector #7
(2 inches downstream from Injector)

Figure 17: Comparison of Averaged Fuel Mass Flux Computations and Measurements 2-inches Downstream of Injector #7

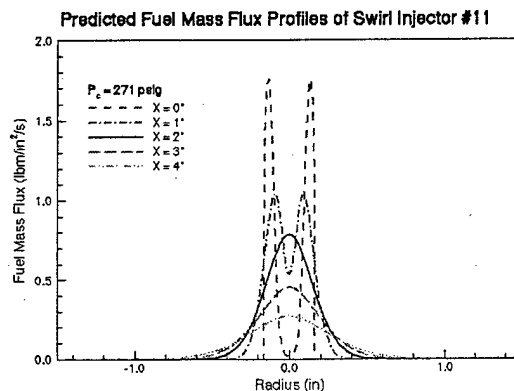**Predicted Fuel Mass Flux Profiles of Swirl Injector #11**

Figure 15: Averaged Mass Flux of Fuel Profile at Various Axial Locations for Injector #11

Comparison of Fuel Mass Flux Distribution of Swirl Injector #11
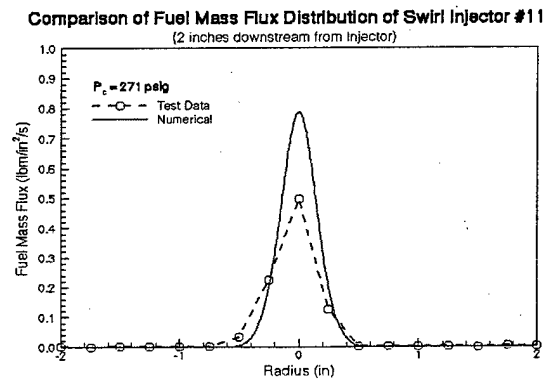(2 inches downstream from Injector)

Figure 18: Comparison of Averaged Fuel Mass Flux Computations and Measurements 2-inches Downstream of Injector #11
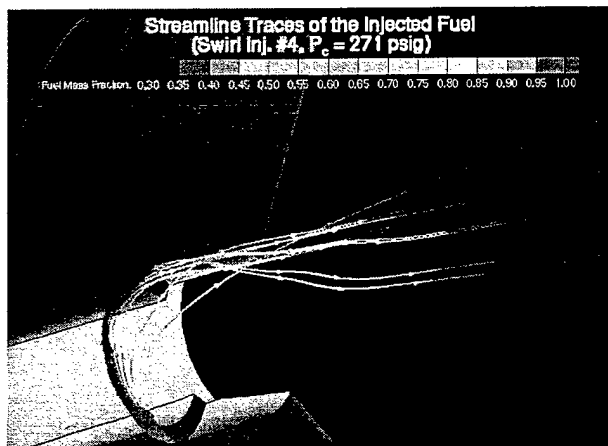
7

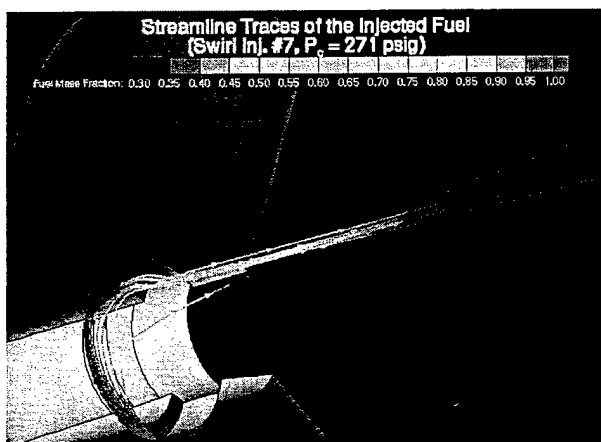**Figure 19: Streamline Traces of the Injected Fuel for Injector #4**

Figure 20: Streamline Traces of the Injected Fuel for Injector #7
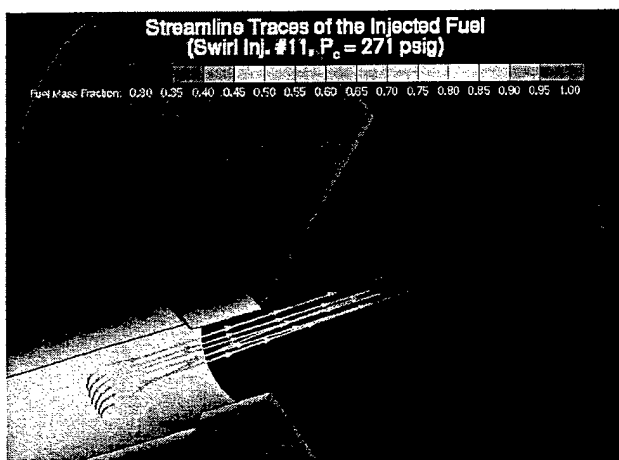

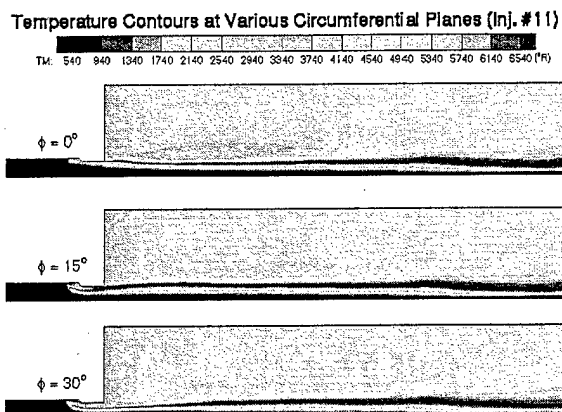**Figure 21: Streamline Traces of the Injected Fuel for Injector #11**

Figure 22: Predicted Temperature Contours for Various Circumferential Planes for Injector #11 Uni-Element Hot-Fire Operation
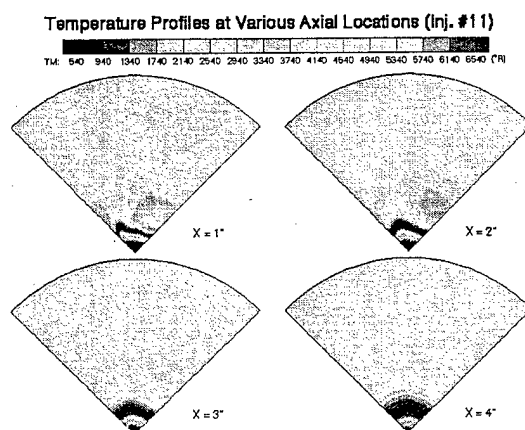

Figure 23: Predicted Temperature Contours at Various Downstream Axial Locations for Injector #11 Uni-Element Hot-Fire Operation
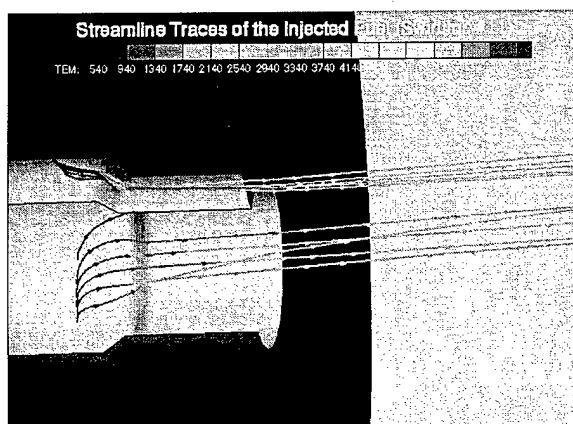

Figure 24: Fuel Streamlines within Injector #11 for Uni-Element Hot-Fire Operation

8

Temperature Contours & Velocity Vectors at the Symmetry Plane
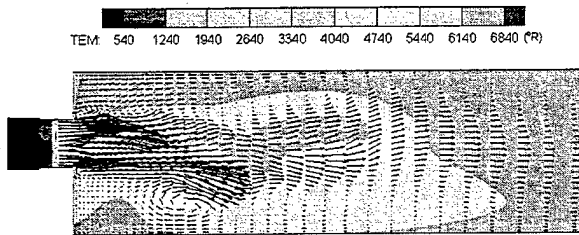of an Injector (1000 psi)

TEM: 540 1240 1940 2640 3340 4040 4740 5440 6140 6840 (°R)

Figure 25: Predicted Temperature Contours and Velocity Vectors AFT Operation at PC=1000 psi

Temperature contours at a radial plane through injector center

TEM 540 1160 1780 2400 3020 3640 4260 4880 5500 6120 6740
P_c = 1000 psi

Figure 26: Near-Face Temperature Distribution for AFT Operation at PC=1000 psi

O2: 0 0.1 0.2 0.3 0.4 0.5 0.6 0.7 0.8 0.9 1
P_c = 2000 psi

Figure 27: Near-Face Oxygen Fraction Distribution for AFT Operation at PC=1000 psi. Stoichiometric Ox Fraction~0.75

Temperature Contours & Velocity Vectors at the Symmetry Plane
of an Injector (2000 psi)

TEM: 540 1240 1940 2640 3340 4040 4740 5440 6140 6840 (°R)

Figure 28: Predicted Temperature Contours and Velocity Vectors AFT Operation at PC=2000 psi

Temperature contours along a radial plane through the injector center

TEM: 540 1160 1780 2400 3020 3640 4260 4880 5500 6120 6740
P_c = 2000 psi

Figure 29: Near-Face Temperature Distribution for AFT Operation at PC=2000 psi

O2: 0 0.1 0.2 0.3 0.4 0.5 0.6 0.7 0.8 0.9 1
P_c = 1000 psi

Figure 30: Near-Face Oxygen Fraction Distribution for AFT Operation at PC=1000 psi. Stoichiometric Ox Fraction~0.75

9

Figure 31: Radial Temperature Profiles for AFT Operation at PC=1000 psi

Figure 33: Radial Temperature Profiles for AFT Operation at PC=2000 psi

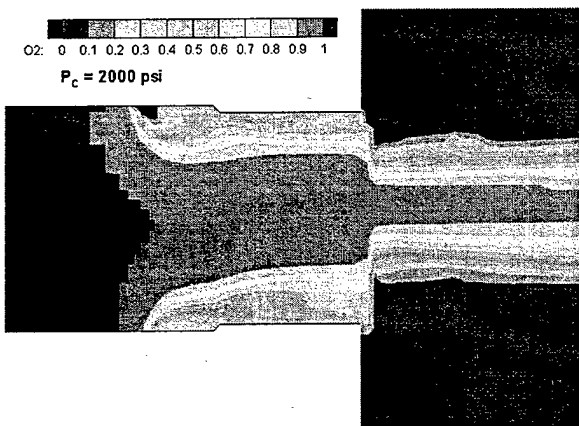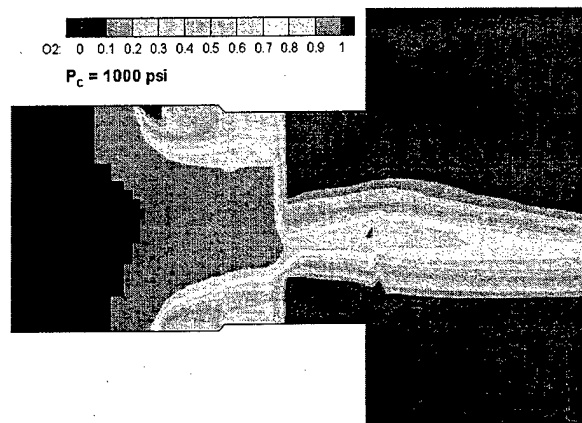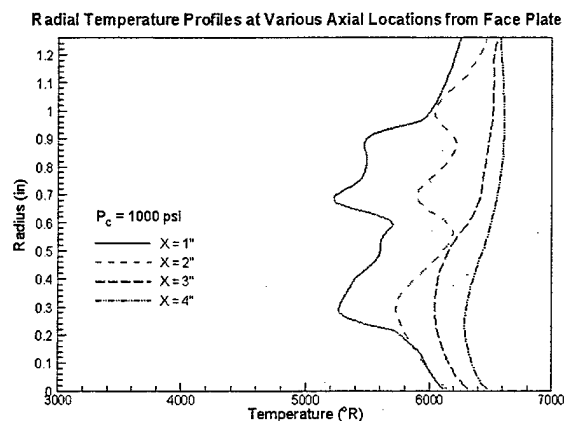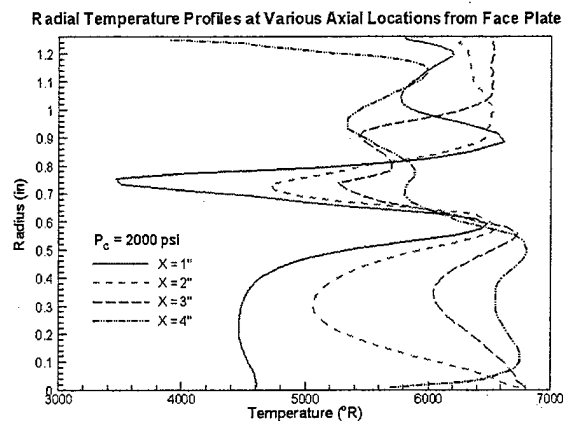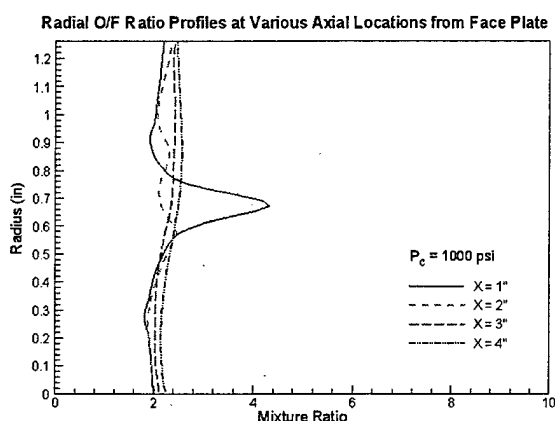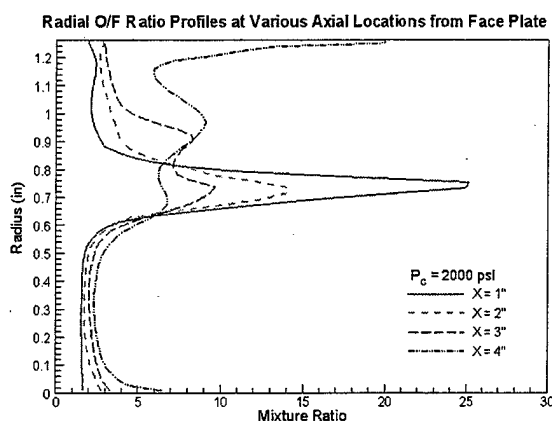Figure 32: Radial O/F Mixture Ratio Profiles for AFT Operation at PC=1000 psi

Figure 34: Radial O/F Mixture Ratio Profiles for AFT Operation at PC=2000 psi

Discussion

Comparison of the cold flow uni-element CFD simulation results with the test data shows that the model picks up the major flow phenomena and trends measured in the cold flow tests. Figure 35 illustrates that the analysis predicts the same order of peak fuel mass flux as measured in the cold flow experiments for the 3 injectors (Injectors #4, #7, and #11). The relative differences in peak mass flux are well predicted by the model, and the simulation also appears to match the spray fan angle.

The limited spatial resolution of the measured mass-flux data makes it is impossible to determine if the lobed structure predicted by the simulations for Injectors #4 and #7 is present in the cold flow experiment. Integration of the cold flow fuel flux results for Injectors #4 and #7 greatly under-estimate

total water flow, suggesting such a structure may have occurred, but may have been missed by the coarse patternator. In contrast, integration of the cold flow fuel flux for Injector #11 shows a smaller under-estimation, supporting that the absence of the lobed structure predicted by the CFD simulations.

Some simplifying assumptions contained within the CFD model may introduce errors in the cold flow numerical analysis. One possible source of error in the analysis is the homogenous spray model employed by the FDNS-RFV code. Propellant mixing is predicted using a turbulence model that was tuned for incompressible flows. Additionally, all operating chamber pressures are much lower than the critical pressure of water, while the simulation assumes the presence of a single fluid phase. Thus the cold flow test flowfield is subjected to the subcritical spray condition where inter-phase effects, such as droplet

10

atomization, droplet/turbulence interaction and momentum lag, are very important. The homogeneous spray model, which assumes the particulate phase and the gas phase to be in equilibrium (i.e. no lag in momentum and heat transfer), is suitable for spray at the supercritical or near the critical condition. The result is that the predicted propellant mixing is likely in error for sub-critical water. It should be noted that liquid rocket engines operate at high supercritical condition, therefore the water/gN_2 injector cold flow test may not reasonably emulate the injector flow in real rocket engines. However, the favorable comparison of mixing trends between the CFD analysis and the cold flow tests provides confidence that the CFD analysis can be an effective tool in injector design.
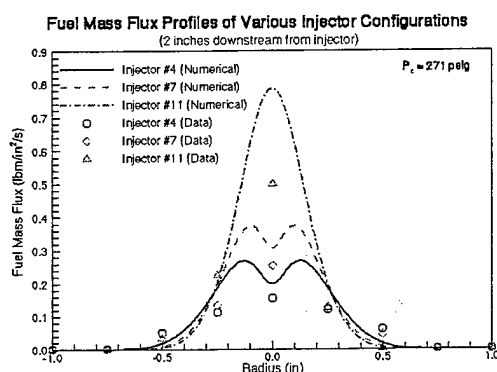

Fuel Mass Flux Profiles of Various Injector Configurations
(2 inches downstream from injector)

Figure 35: Averaged Fuel Mass Flux Profiles of Various Injector Configurations

Effects of Geometry

The contour and streamline profiles demonstrate the physics behind the mixing in these elements. The swirling fuel creates an annulus of fuel on the inner wall of the bottom portion of the GOX post. The combination of the tangential fuel flow and shear of the fuel by the strong axial oxidizer flow results in a cylindrical sheet of fuel, which cools the GOX post wall near the post exit. As the fuel leaves the post, the sheet breaks into droplets and tends to be pushed away from the center flow. As the fuel travels away from the injector face, the fuel gets entrained into the GOX flow.

The above description of injector operation would suggest that the geometry in the tip region play an important role in mixing efficiency. For example, a smaller GOX post diameter creates faster GOX velocity, thereby increasing entrainment (as can be

seen in results for Injector #11). The fact that the mean oxidizer velocity is slowed as it diverges may explain why Injector #4 does not mix as quickly as the other elements. The diverger design also includes a 5 mil dead zone between the incoming fuel jets and the central oxidizer core. While this gap was included to facilitate formation of a liquid sheet, it also delays interaction between the fuel and oxidizer and their subsequent mixing and reaction. Uni-element hot-fire performance trends support this hypothesis[1]. Continued parametric experimentation on the diverger element design, coupled with additional CFD simulations should permit a better understanding of the relationship between tip geometry and injector performance.

Though optimized mixing efficiency is the goal of the injector design, the rapid mixing may result in local overheating of the injector post under hot-fire conditions. Moreover, differences between the hot-fire and cold flow conditions are expected due to combustion related effects. However, Cold-flow spray injection is an extremely useful tool in gaining insight into injector performance.

Effects of Chamber Pressure

The effect of chamber pressure (Pc) on mixing efficiency was examined for both the uni-element cold flow and the multi-element AFT configurations. Cold flow simulations and tests fuel mass flux profiles are shown for Injector #11 in Figure 36. Both data and simulation indicate that chamber pressure does not have a strong effect on the liquid propellant distribution, and thus the mixing efficiency. Additionally there is good consistency between the simulations and the cold flow test data. These results also suggest that this injector element should perform well under throttled conditions.
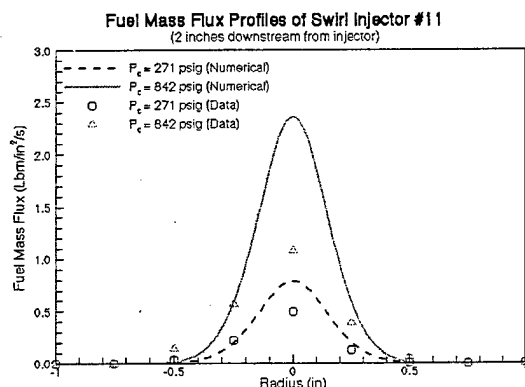
11

American Institute of Aeronautics and Astronautics

Figure 36: Averaged Fuel Mass Flux Profiles for Injector #11 at Pc = 271 and 842 psig

Conclusions

Comparison of the cold flow measurements to the CFD analysis suggests that FDNS is capable of capturing major trends in mixing phenomenon for these gas-centered swirl coaxial elements. Consequently the CFD simulations can aid in design of the injector by both qualitatively identifying design sensitivities and quantitatively validating experimental results. Specifically, the analysis predicts the same order of peak water mass flux as measured in the cold flow experiments for different injector geometry configurations. The analysis predicts the solid cone spray distribution consistently measured during the cold flow tests.

The homogeneous spray model in FDNS is not completely consistent with the cold flow analysis since the model assumes the inter-phase effects (surface tension and momentum lag) to be negligible in a supercritical mixture. Thus the assumption of supercritical fluid in phase equilibrium was not met for the cold flow test with water. However, the results show that the homogeneous spray model is sufficient to make relative comparisons between different injectors. The model is expected to be quantitatively more accurate for the supercritical conditions existing in the real combustion process.

The model identifies the physical phenomena producing the mixing in these elements. The elements swirl the fuel around the inside of the GOX post. That fuel is swept out of the GOX post in a sheet and then entrained into the high velocity GOX flow downstream of the element. However, sufficient simulations have not been completed to determine the sensitivity of the mixing to major design parameters, such as GOX velocity, fuel swirl, and injector geometry. The simulations completed suggest that the

models are capable of providing meaningful results for these types of parametric studies.

Future Work

The data presented suggests that CFD simulations can identifying valuable relationships between injector geometry and operating conditions and the resultant performance. Further simulations will be performed to support evaluation of new injector design evolutions, including large thrust elements for National Aerospace Initiative.

The simulation results presented here need to be compared to the uni-element hot-fire testing and multi-element AFT test data when available. These data will validate the utility of FDNS as a key component in the design of high-performance rocket combustion chambers. A validated simulation tool is invaluable for predicting near-face and wall boundary conditions, which in turn are primary drivers in determining engine life and reliability.

Acknowledgements

References

1. Muss, J.A., Johnson, C.W., Cohn, R.K., Strakey, P.A., Bates, R.W. and Talley, D.G., "Swirl Coaxial Injector Development Part I – Test And Results", 38th JANNAF Combustion Subcommittee Meetings, Destin, FL, April 8-12, 2002

2. Cheng, G.C. and Farmer, R.C., "CFD Spray Combustion Model for Liquid Rocket Engine Injector Analyses," AIAA Paper 2002-0785.

3. Cheng, G.C., Anderson, P.G., and Farmer, R.C., "Development of CFD Model for Simulating Gas/Liquid Injectors in Rocket Engine Design," AIAA Paper 97-3228, 1997.

4. Farmer, R.C., Cheng, G.C., Trinh, H., and Tucker, K., "A design Tool for Liquid Rocket Engine Injectors," AIAA 2000-3499, 2000.

12

5. Chen, Y.S., "Compressible and Incompressible Flow Computations with a Pressure Based Method," AIAA Paper 89-0286, 1989.

6. Hirschfelder, J.O., et al, "Generalized Equations of State for Gases and Liquids," IEC, 50, pp.375-385, 1958.

7. Hirschfelder, J.O., et al, "Generalized Excess Functions for Gases and Liquids," IEC, 50, pp.386-390, 1958.

8. Reid, R.C., et al, The Properties of Gases & Liquids, 4th ed., McGraw-Hill, 1987.

9. Gordon, S., and B.J. McBride, "Computer Program for Calculation of Complex Chemical Equilibrium Compositions, Rocket Performance, Incident and Reflected Shocks, and Chapman-Jouget Detonations," NASA-SP-273, 1971.

10. Saad, Y., and Schultz, M.H., SIAM Journal of Sci. Stat. Comput., Vol. 7, pp. 856-869, 1986.

11. Johnson, C.W., Muss, J.A., Cheng, G.C. and Farmer, R.C.; "Characterization of GOX/Kerosene Combustor Performance Through Plume Diagnostics ", JANNAF Combustion Sub-committee Meeting, Monterey, CA, Nov. 2000.

12. Cheng, G.C., Johnson, C.W., Muss, J.A., and Cohn, R.K., "Swirl Coaxial Injector Development, Part II: CFD Modeling," 2002 JANNAF CS/APS/PSHS/MSS Joint Meeting, Destin, FL, April 2002.

Table 1: Kinetic Chemistry Model for RP-1/O2 Reaction[4]

QUASIGLOBAL KINETICS MODEL WITH SOOT FORMATION				
Global Mechanism	A	B	E/R ($^\circ$K)	Power Dependencies (γ_j)
RP-1 Pyrolysis $C_{12.4}H_{24.8} \rightarrow 6.2\ C_2H_4$	3.0117 E10	0	2.523E4	$[C_{12.4}H_{24.8}]^{0.5}$
Oxidation of Pyrolysis Gas $C_2H_4 + O_2 \rightarrow 2\ CO + 2\ H_2$	1.2900 E15	1	2.5160 E4	$[C_2H_4]^{0.5}[O_2]^{1.0}$
Soot Formation $48\ C_2H_4 \rightarrow C_{96}H_{24} + 84\ H_2$	5.1308E12	-2	1.6110 E4	$[C_2H_4]^2[O_2]^{-0.5}$
Note: $\quad [\dot{C}_i] = AT^B \exp\{-E/RT\}[C_j]^{\gamma_j}$ $[C_j]$: concentrations (gm moles/cm^3)				

SOOT OXIDATION MODEL
Soot + 48 $O_2 \rightarrow$ 96 CO + 12 H_2

$$\text{Rate} = \frac{72\,M_{w_s}\,R_u\,T}{\rho_s\,D_s}\left[\frac{K_1\,\psi}{1+K_4\,P_{O_2}} + K_2\,(1-\psi)\right][\text{Soot}][O_2]$$

$$\text{where } \psi = \left(1 + \frac{P_{O_2}\,K_3}{K_2}\right)^{-1} ; \quad K_i = A_i\,e^{\frac{-E_i}{R\,T}} ; i = 1 \rightarrow 4$$

$A_1 = 20$, $E_1/R = 1.509 \times 10^4$

$A_2 = 4.46 \times 10^{-3}$, $E_2/R = 7.6497 \times 10^3$

$A_3 = 1.51 \times 10^5$, $E_3/R = 4.8817 \times 10^4$

American Institute of Aeronautics and Astronautics

$A_4 = 21.3,$	$E_4/R = -2.0634 \times 10^3$

$R_u = 82.06$ atm@cm^3/g-mole@°K

ρ_s (density of soot) = 1.86 g/cm^3

D_s (diameter of soot) = 40 nm (assumed value)

M_{w_s} (molecular weight of soot) = 1177.25 g/g-mole

P_{O_2} (partial pressure of O_2, in atm)

Note: Soot is defined as $C_{96}H_{24}$ in order to treat it as an idea gas. This approximation makes incipient soot particles the right size and maintains the right carbon-to-hydrogen ratio for soot.

Wet-CO Mechanism			
Reaction	A	B	E/R
$H_2 + O_2 \equiv OH + OH$	1.7000E13	0	2.4070E4
$OH + H_2 \equiv H_2O + H$	2.1900E13	0	2.5900E3
$OH + OH \equiv O + H_2O$	6.0230E12	0	5.5000E2
$O + H_2 \equiv H + OH$	1.8000E10	1.0	4.4800E3
$H + O_2 \equiv O + OH$	1.2200E17	-0.91	8.3690E3
$M + O + H \equiv OH + M$	1.0000E16	0	0
$M + O + O \equiv O_2 + M$	2.5500E18	-1.0	5.9390E4
$M + H + H \equiv H_2 + M$	5.0000E15	0	0
$M + H + OH \equiv H_2O + M$	8.4000E21	-2.0	0
$CO + OH \equiv H + CO_2$	4.0000E12	0	4.0300E3
$CO + O_2 \equiv CO_2 + O$	3.0000E12	0	2.5000E4
$CO + O + M \equiv CO_2 + M$	6.0000E13	0	0

American Institute of Aeronautics and Astronautics